Dual-tunable phononic waveguides for manipulation of guided Lamb waves

Wei Guo *,[1] Yu-Ke Ma *,[1] Yan-Feng Wang,[1,†] Vincent Laude,[2] and Yue-Sheng Wang[1,3]

[1]*School of Mechanical Engineering, Tianjin University, 300350 Tianjin, China*

[2]*Université de Franche-Comté, CNRS, Institut FEMTO-ST, F-25000 Besançon, France*

[3]*Institute of Engineering Mechanics, Beijing Jiaotong University, Beijing 100044, China*

In this paper, we design and fabricate dual tunable waveguides in a two-dimensional periodic plate with threaded holes. Dual tunability is realized by using rods held with nuts as well as assembly prestress of the nuts. A straight waveguide, a bent waveguide and a wave splitter are designed by changing the distribution of rods and nuts in different circuits. The experimental and numerical results show that the frequencies of guided waves can be tuned by the assembly prestress. By increasing the amount of prestress, the frequency range of the passing band can be shifted upward. Confinements, guiding and splitting of Lamb waves are clearly observed in both experimental measurements and numerical simulations. This work is essential for the practical design of reconfigurable phononic devices.

I. INTRODUCTION

As artificially periodic composites, phononic crystals (PCs) have been attracting more and more attention for the last 3 decades[1]. They can exhibit bandgaps in certain frequency ranges, within which the propagation of acoustic or elastic waves is prohibited[2]. Generally, there are two main mechanisms for bandgap generation: Bragg scattering and local resonance[3,4]. Bragg bandgaps are mainly dependent on the structural periodicity. The corresponding wavelength is in the same order with the lattice constant. While in contrast resonant bandgaps are mainly dependent on the resonance of the scatterers. The wavelength inside the bandgap is much larger than the lattice constant. The nature of bandgaps can be used for vibration reduction[5–7], and sound isolation[8–10].

* Wei Guo and Yu-Ke Ma contributed equally to this work.

When one or some scatterers are removed or replaced with different shapes or materials, the periodicity of PCs is broken. Defected states are then induced inside the bandgap[11–13] and can be used to design novel wave devices. Point, linear and planar defects can be obtained by modifying one, one line or one layer of scatterers. Wave or energy can be trapped around the point defect, so point defects might be applied for the design of novel cavity[14,15] or energy harvester[16,17]. A linear defect can be used to confine the energy around the defect and guide the propagation of energy. So they can be used to design waveguides[18,19]. This can also be realized by using a linear chain of point defects[20]. Planar defect introduces modes with energy localized in the plane[21]. Combination of different defects can be used to design various wave devices, such as filter, coupler, splitter and frequency demultiplexer[22–24].

Despite the existence of the above wave behaviors, practical applications of PCs are rarely demonstrated because the operating frequency ranges of the PC-based devices are generally fixed. The concept of tunable PCs has thus been developed as a separate research field[25]. Generally, there are two main regulation mechanisms. On the one side, tunable PCs are realized by physically adjusting the material parameters. Such systems generally consist of multiphysics coupled media, which are sensitive to the electric field[26–28], magnetic field[29–31], optical field[32] and thermal field[33–35]. On the other hand, tunable PCs are realized by mechanically changing the geometrical topology. In addition to filling fluid in PCs with blind holes[36,37], prestress is commonly used to tune wave propagation. Apart from granular PCs[38,39], the related investigations on the continuous prestressed PCs generally include two parts.

First, some investigations focus on PCs with traditional elastic materials. Gei et al investigated flexural wave propagation in the prestressed periodic beam on an elastic foundation[40]. They showed that bandgaps can be shifted upward (downward) for tensile (compressive) prestress. Wang et al. calculated the effects of prestress on the bandgaps of three-dimensional pizeoelectric phononic crystals[41]. The location of bandgaps was found to increase with increasing prestress, while the width of bandgap remains almost unchanged. Zhu et al studied the bandgap adjustability under prestretch strain[42]. Applying prestretch strain to the matrix can realize active realtime control of low-frequency bandgap under slight deformation and broaden the low-frequency bandgap. Li et al showed that the frequency ranges of nonreciprocal transmission can be shifted down for elastic waves propagating in the combination of nonlinear material and elastic metamaterials with increasing prestress[43]. Large stresses,

however, are required for significant tunability of the elastic materials[44].

Second, some investigations considered PCs with hyperelastic materials. Compared to their elastic counterparts, hyperelastic materials generate large deformation even under a small stress. Bertoldi's group has investigated wave propagation in several soft porous PCs under prestress[45,46]. Novel configuration patterns based on the instability and bulking provides rich room to tune the wave behaviors[47]. Sharma et al. introduced the optimum topologies of the soft compressible unit cells for varying levels of the applied prestretch as well as the longitudinal prestress[48]. They observed that increasing the lateral prestretch together with applying a compressional longitudinal prestress have favorable impact on widening the bandgaps. Bayat and Gordaninejad formed wrinkles in 1D prestressed PC slab composed of a thin soft film attached to a thick substrate[49]. The bandgaps were adjusted by surface instability. Chen et al. realized a tunable soft acoustic diode in the bandgap by changing the applied force[50]. De Pascalis et al. employed genetic algorithm to optimize prestressed phononic media for the low frequency bandgaps of antiplane elastic waves[51]. Miniaci et al. found a remarkable shift of dispersion curves for inertial amplified PCs compared to Bragg or resonant ones[52]. More related work may be found in the recent review[53].

Although there is a lot of literature on prestressed PCs, investigations on the defected PCs are rarely reported[54], especially for Lamb waves. Manipulation of Lamb waves by PCs combining prestress and defects remains a difficult task. In this paper, we design and fabricate dual tunable waveguides in a two-dimensional periodic plate with threaded holes. Dual tunability is realized by using rods held with nuts as well as assembly prestress of the nuts. Guided waves can be tuned by adusting the distribution of rods and nuts in different circuits and controling the amount of assembly prestress. Straight waveguide, bent waveguide and wave splitter are designed by changing the distribution of rods and nuts in different circuits. The frequencies of guided waves are tuned by the assembly prestress. Confinement, guiding and splitting of Lamb waves are clearly observed in both experimental measurements and numerical simulations. This work is important for the design of reconfigurable or programmable elastic wave devices.

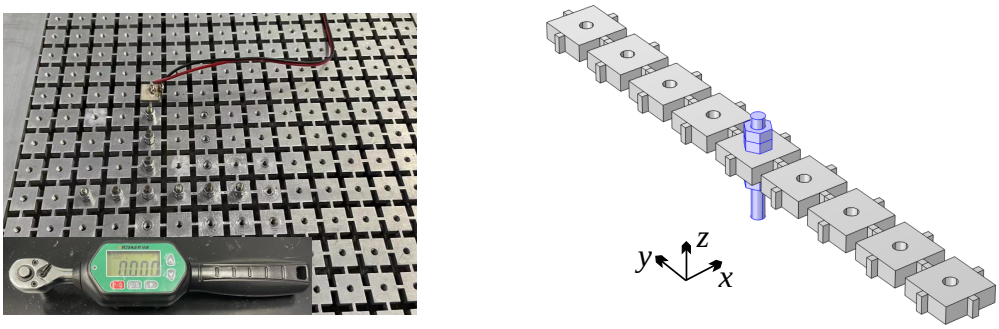

(a) (b)

Figure 1: Dual tunable phononic splitter. (a) Photograph of the wave splitter and the Digital Torque Wrench used to evaluate the assembly prestress. (b) Supercell of waveguide used to calculate the band structure

II. EXPERIMENTAL AND NUMERICAL METHODS

Fig. 1a shows a photograph of the dual reconfigurable phononic splitter fabricated on a PC plate with threaded holes. The splitter is composed of 3 straight waveguides, where the threaded rods are assembled on the plate by 4 nuts placed symmetrically on both sides. The assembly prestress is controlled precisely by a digital torque wrench with 2 % accuracy and 0.2-10 N $\cdot$m range. Note that the exact prestress or prestrain that is applied experimentally is not quantitatively known, though precisely set relatively. An additional benefit of the use of the digital torque wrench is that prestress can be equilibrated on all assemblies to obtain the same resonance frequency for all defects. The asymmetric wave source is excited by the vertically-polarized piezoelectric patch glued on one side of the plate, which excites Lamb waves. And the piezoelectric patch is positioned away from the edge of the plate, minimizing the inference of reflected waves on the experimental results. Experimental measurements are conducted by using Polytec PSV-500 scanning vibrometer. Transmission properties and displacement distribution of waveguides are measured by considering harmonic excitation with stepped or fixed frequencies. The signals are amplified before being applied to the piezoelectric patch. The excitation source is asymmetric with respect to the mid-plane of the plate, which is beneficial to the excitation of out-of-plane modes. However, due to the finite lateral extent of the source[55], in-plane modes may be excited as well.

Numerical simulations are conducted by using the finite element software COMSOL. The assembly prestress is taken into account through prestrain in the Solid Mechanics Module. Before solving for the band structures or transmission properties of the structures, a sta-

tionary study is performed to calculate the static deformation of the structure under the prestress. The geometrical and material parameters of the plate, rods and nuts are exactly the same with those in Ref.[56]. Fig. 1(b) illustrates the supercell of the waveguide used for the calculation of band structures. The plate is divided into 4 parts in the thickness direction. Quadratic serendipity element is applied to approximate the displacement field. Periodic Bloch bondary conditions are applied along the x and y directions, and the other surfaces are set as traction-free. The band structure is obtained by sweeping the wave vector along the irreducible Brillouin zone of the supercell. Eigenmodes at the marked points are also obtained by choosing the suitable wavenumber and frequency. In addition, the polarization amounts for the out-of-plane modes are calculated based on the eigenmodes. They represent the contribution of out-of-plane displacements to the total polarization of elastic waves.

Transmission properties are evaluated by considering a 3D plate model. An asymmetric wave source is applied to the top of the plate. The response is collected in the region S_1 (with the area A_1) on the end of the waveguides. We define the numerical transmission as

$$F = 20\log_{10}\left(\frac{\int_{S_1} |U_1|/A_1 dS}{|U_0|}\right), \tag{1}$$

where $U_0 = 1$ is the amplitude of the z-polarized wave source and U_1 is the total displacement received on the end of the waveguides (S_1).

III. RESULTS AND DISCUSSIONS

In this section, we discuss the band structures and transmission properties of dual tunable waveguides with different prestress.

A. Defect modes of prestressed waveguides

First we investigate the band structures and defect modes of prestressed waveguides. The supercell is shown in Fig. 1(a). For comparison, we also consider the phononic waveguides assembling by rods and nuts with perfect bonds. Band structure of the waveguide with perfect bond is presented in Fig. 2(a), together with the vibration modes of the defected

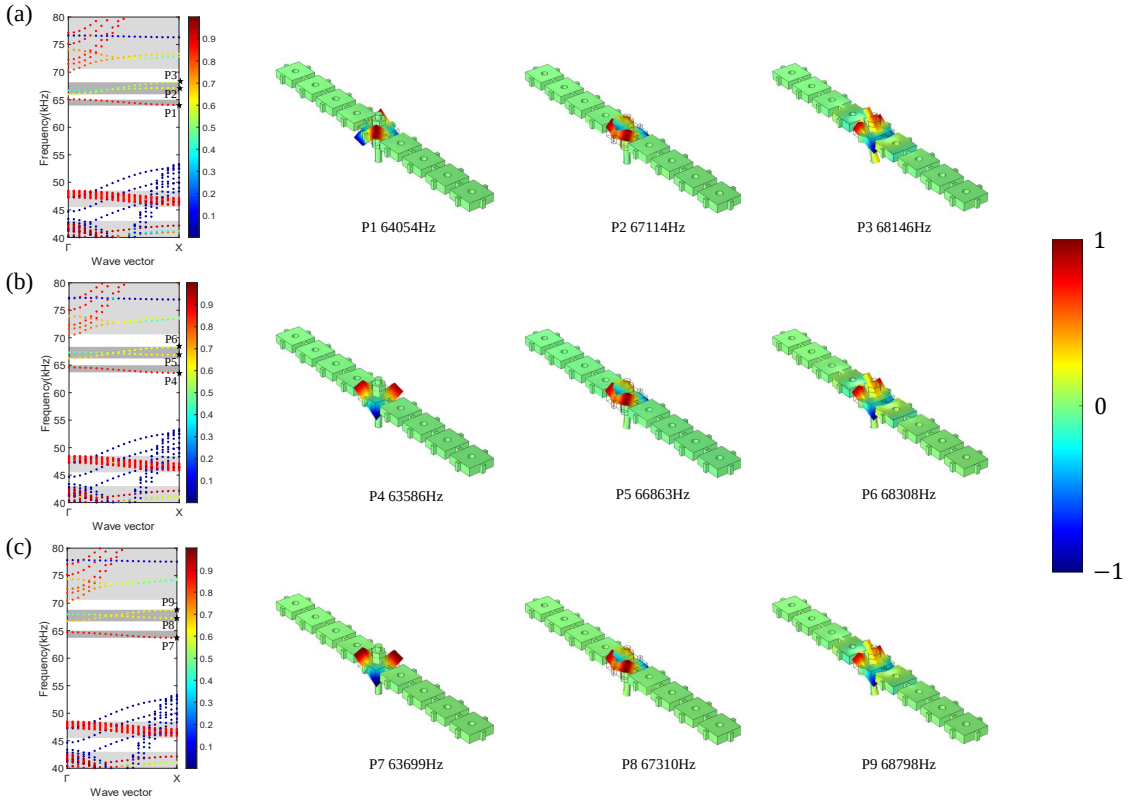

Figure 2: Band structures and vibration modes of the phononic waveguides with perfect bonds (a) or different prestrains: (b) 0.0083 and (c) 0.0167. The color scale represents the polarized amount from 0 (blue) to 1 (red). The light-gray areas indicate the passing band for the out-of-plane polarized waves in the perfect PC slab. The dark-gray areas indicate the considered frequency range of guided bands. Vibration modes at marked points are shown on the right. The color scale represents the normalized amplitude of out-of-plane displacements from -1 (blue) to 1 (red).

bands in the marked points. It is observed that the band structure is different from that in[56] because two nuts are added on both sides of the plate. This also indicates the reconfigurability of the proposed waveguide. The defect mode at point P1 is flexural-dominated but asymmetric with respect the wave propagation direction. So it is a deaf mode and can not be excited by a symmetric plane wave. This also holds for the defect mode at point P3. So only the defect mode at point P2 contributes to the transmission.

Figs. 2(b) and (c) show the band structures and vibration modes of the phononic waveguides with different prestrains. The two coupled defect bands shift upward with increasing prestrain. It seems, however, that the band structures and the bandgaps do not change significantly when prestrain is applied. This can be quantitatively identified by observing the eigenfrequency of the marked points. The vibration modes of the defect bands are sim-

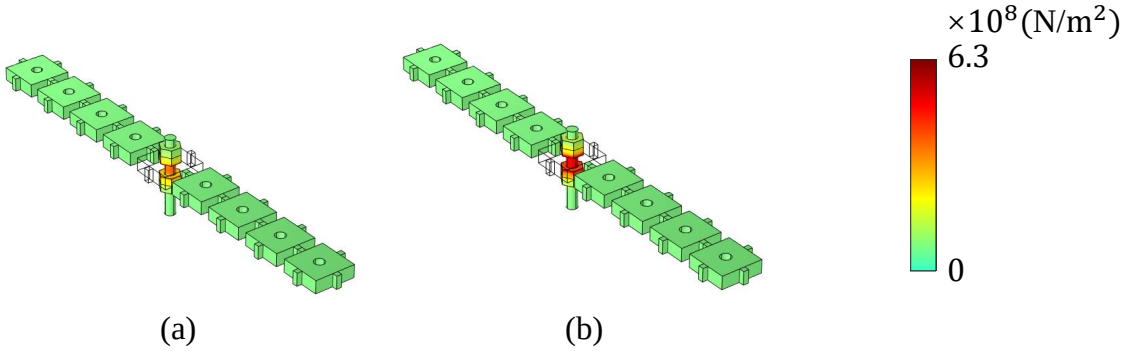

Figure 3: Von Mises stress distribution of the supercells with different prestrains: (a) 0.0083 and (b) 0.0167. The structures around the rods are hidden. The color scale represents the stress amount from 0 (green) to 6.3×10^8 (red).

ilar to the case with perfect bond. The defect band around 65 kHz is almost independent of the prestrain because the threaded rod feels almost no vibrations, see the corresponding vibration modes at points P4 and P7. The vibration is asymmetric with respect to the wave propagation direction, so these two bands are deaf. This also holds for points P6 and P9. Only the guided modes P5 and P8 contribute to the transmission.

It is noted that the adjustment of prestress has a range. The stress of the rods cannot exceed the yield limit. Figs. 3(a) and Figs. 3(b) show the von Mises stress distribution of the structures with different prestrains. It is found that the stress is mainly concentrated on the rods. Under the two prestrains, the maximum von Mises stress in the rods are 3.4×10^8 and 6.3×10^8 N/m^2, respectively. They are all within the yield limit of the material, which is 6.9×10^8 N/m^2[57–59].

The above analysis shows that the defect bands appearing in the band gaps are sensitive to the prestrains. Waveguiding at different frequencies thus can be tuned by changing either the prestrains applied on the nuts or the geometric pattern of the defects.

B. Straight waveguide

In this subsection, we focus on wave propagation in straight waveguides with a length of 7 units. The simulation results for the transmission spectrum under different prestrains are given in Figs. 4(b)-(c). The result for perfect bond is given in Fig. 4(a). Three passing bands are clearly observed above 67 kHz. Their frequencies increase with increasing prestrain, consistently with the band structures shown in Fig. 2. The transmission modes

at the marked points of the transmission spectrum are given in Fig. 4 (d). Elastic waves are clearly guided by the linear defects. It is also noted that the transmission around 65 kHz is relatively small, since the corresponding band is deaf. The experimental transmissions for

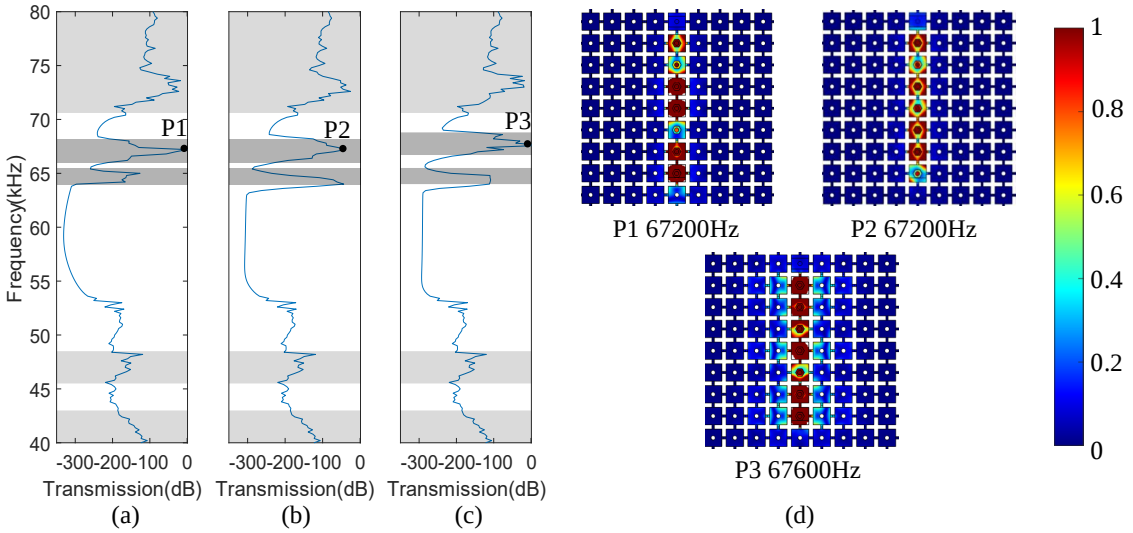

Figure 4: Simulated transmissions of the straight waveguides with perfect bonds (a) or different prestrains: (b) 0.0083 and (c) 0.0167. Vibration modes at the corresponding labeled points are given in panel (d). The color scale represents the normalized amplitude of out-of-plane displacements from 0 (blue) to 1 (red).

the straight waveguides are given in Fig. 5 for different prestrains (represented by torques measured by the Digital Torque Wrench). It can be observed that transmission near 67 kHz is apparent when the magnitude of the torque is 2.3 $\mathrm{N}\cdot\mathrm{m}$. It gets more pronounced with increasing torque. The transmission modes at the labeled points are given in Fig. 5(d). It can be observed that vibrations are clearly confined and guided along the linear defects around 67 kHz. These results are consistent with the numerical ones in Fig. 4. It is also noted that there are passing bands around 57 kHz in the experimental spectrum. They correspond to the passing band around 53 kHz in the numerical spectrum. Fig. 2 shows that the modes around 53 kHz are the result of the coupling of in-plane and out-of-plane modes. Although the bands in Fig. 2 are in-plane dominated, the coupled modes are excited in the experiments for the asymmetric excitation, see the vibration modes around 57 kHz in Fig. 5(d). Due to the coupling of the modes, the causes of frequency shift are complicated. In addition, there are other differences between numerical results and experimental measurements. When screwing the nuts in the experiments, it cannot be guaranteed that the force exerted by the nut on the rod is uniformly acting on the force area of the rod, which is not accounted

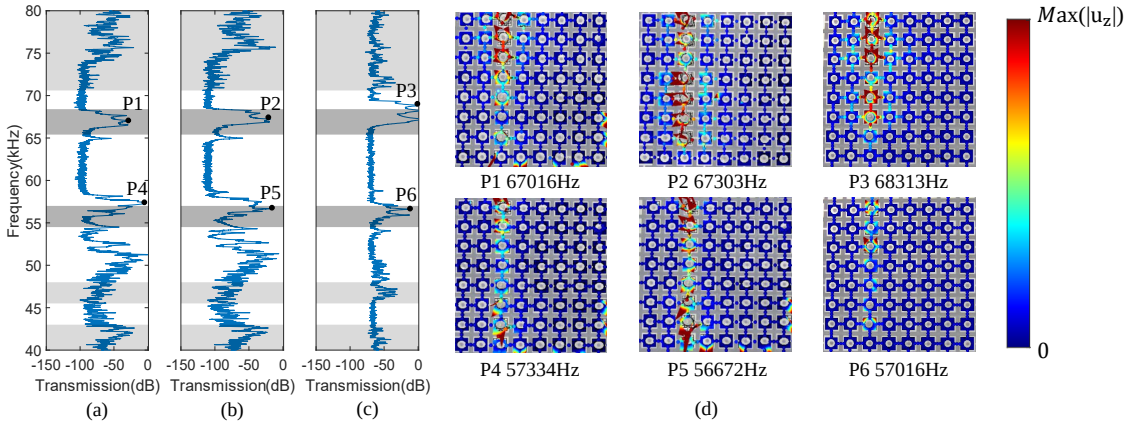

Figure 5: Measured transmissions of the straight waveguides with different torques: (a) 2.3 N · m, (b) 2.7 N · m, and (c) 3.0 N · m. Vibration modes at the corresponding labeled points are given in panel (d). The color scale represents the normalized amplitude of out-of-plane displacements from 0 (blue) to maximum (red).

for in the numerical simulation. Besides, the thread structures are not considered in the simulation. The observed differences may be attributed to all these contributions.

C. Bent waveguide

In addition to the straight waveguide, tunability is also feasible for the design of other waveguides, such as waveguides with 90° bend. The bent waveguide is composed of 7 defected units. Transmission of the bent waveguide with perfect bond is given in Fig. 6a. The results with different prestrains are given in Figs. 6b and 6c. It is found that there is a passing band above 65 kHz for the waveguide with perfect bond, the frequency range of which is identical to that of the straight waveguide in Fig. 4a. With the increase of prestain, passing band in the transmission spectrum shift upwards. Fig. 6d shows the displacement distribution at the points marked on the passing bands in the transmission spectrum. Energy is observed to propagate easily through the bend. We further performed experimental measurements on the bent waveguide with different prestresses. The transmission and displacement distributions are shown in Fig. 7. A passing band is clearly found in the transmission spectrum above 65 kHz. With increasing prestress, the passing band moves upward, consistently with the numerical results in Fig. 6. But the frequency ranges do not change too much, possibly due to gap between threaded holes and rods in the experiment. The waveguide phenomenon can be observed in all the displacement fields extracted in the experiment in Fig 7d. A similar

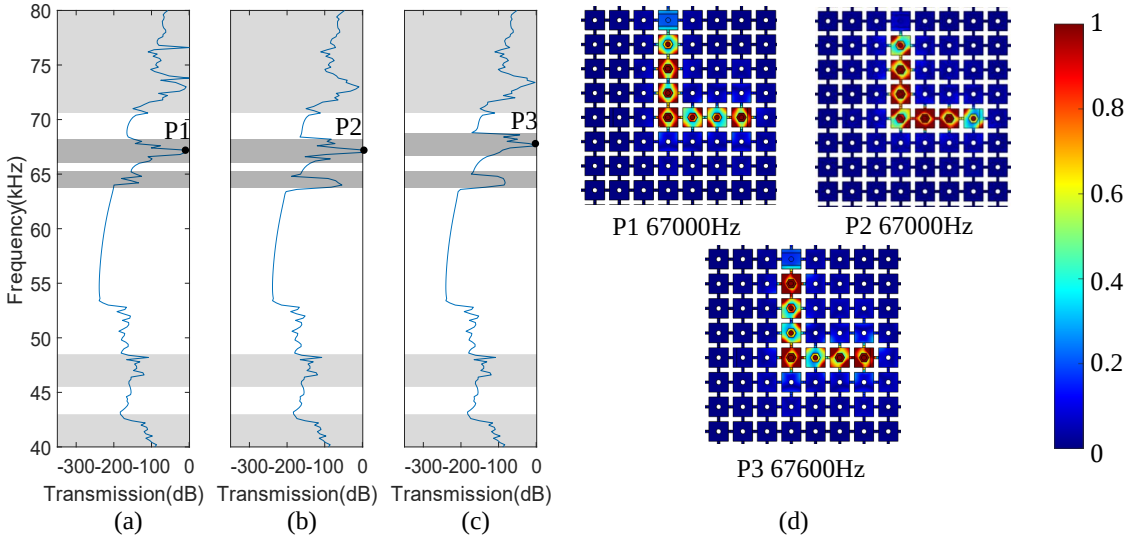

Figure 6: Simulated transmission properties of the bent waveguides (7 units) with perfect bonds (a) or different prestrains: (b) 0.0083 and (c) 0.0167. Vibration modes at the corresponding labeled points are given in panel (d). The color scale represents the normalized amplitude of out-of-plane displacements from 0 (blue) to 1 (red).

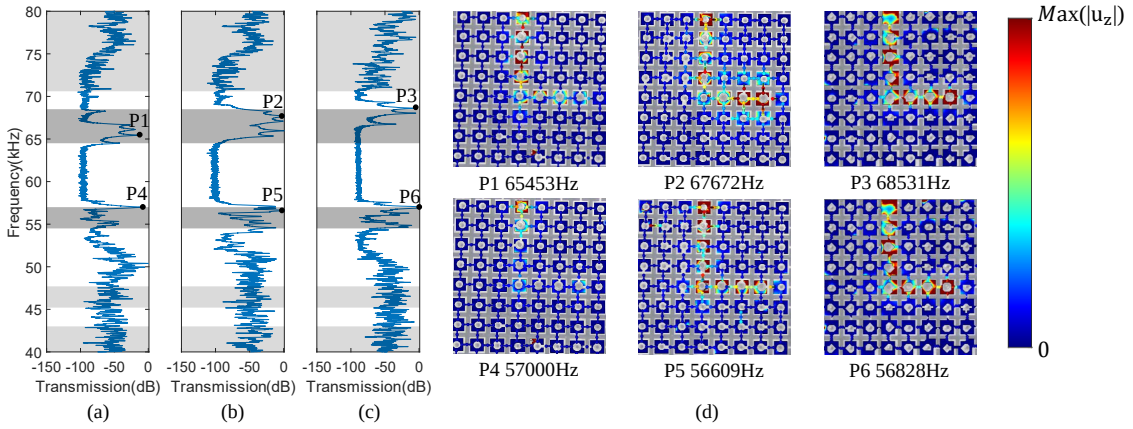

Figure 7: Measured transmissions of the bent waveguides (7 units) with different torques: (a) 2.3 N · m, (b) 2.7 N · m, and (c) 3.0 N · m. Vibration modes at the corresponding labeled points are given in panel (d). The color scale represents the normalized amplitude of out-of-plane displacements from 0 (blue) to maximum (red).

phenomenon is also observed around 55 kHz, identical to the experimental results in Fig. 5 for the straight waveguide.

D. Wave splitter

In addition, we also fabricated a wave splitter in the plate with the aid of reconfigurability. Figs. 8 and 9 give the simulated and experimental transmissions and displacement

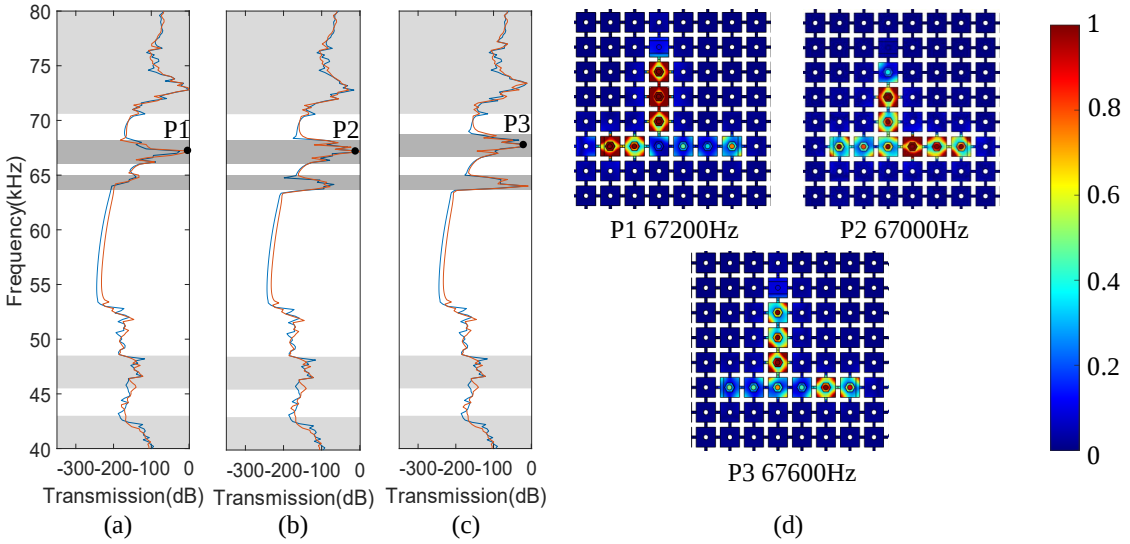

Figure 8: Simulated transmission properties of the wave splitter with perfect bonds (a) or different prestrains: (b) 0.0083 and (c) 0.0167. Transmissions collected on the right and left outputs are marked by blue and red, respectively. Vibration modes at the corresponding labeled points are given in panel (d). The color scale represents the normalized amplitude of out-of-plane displacements from 0 (blue) to 1 (red).

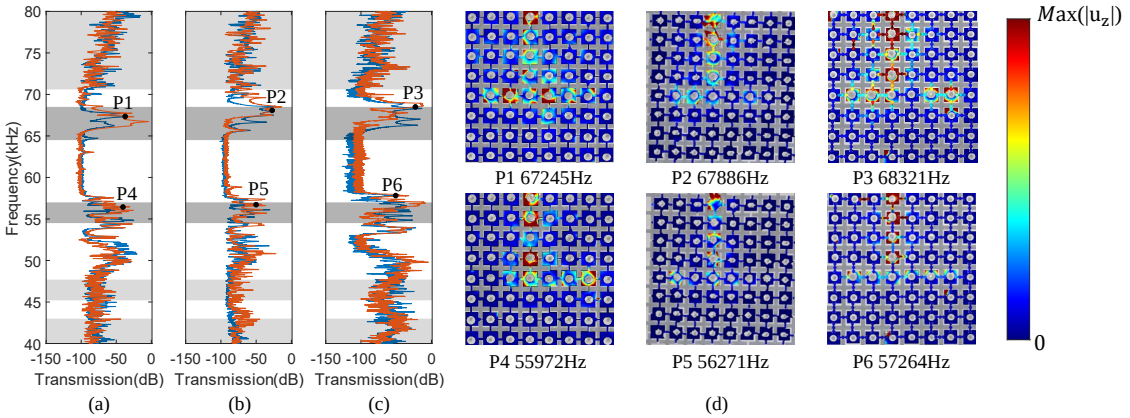

Figure 9: Measured transmissions of the wave splitter with different torques: (a) 2.3 N · m, (b) 2.7 N · m, and (c) 3.0 N · m. Transmissions measured on the right and left outputs are marked by blue and red, respectively. Vibration modes at the corresponding labeled points are given in panel (d). The color scale represents the normalized amplitude of out-of-plane displacements from 0 (blue) to maximum (red).

distributions for wave splitter with different prestrains. The wave source is applied on the top part of the splitter. Transmissions to the left and right output of the splitter are almost identical, suggesting that the wave amplitude is equally split[60]. This also holds for the experimental transmissions in Fig. 9. With increasing prestress, the passing bands in the transmission spectrum shift upward. Wave splitting can be observed in the displacement

fields extracted under the three different prestresses for both simulations and experiments.

IV. CONCLUSIONS

In this paper, we have investigated the manipulation of Lamb waves in dual tunable waveguides formed on a phononic plate. Straight waveguides, bending waveguides and wave splitters were studied. Dual tunability was achieved through the distribution of threaded rods fixed with nuts and the assembly prestress of nuts. Numerical and experimental results show that the introduction of threaded rods with nuts can form different waveguides in the plate and control the wave propagation. By controlling the amount of prestress, the frequency range of the passing band can be adjusted. The larger the prestress, the more the frequency range of the passing band moves toward high frequencies. This phenomenon occurs in both straight waveguides, bending waveguides and wave splitters.

This paper is relevant to the practical application of elastic acoustic devices. With the aid of control elements, the geometric pattern and applied prestress between nuts and plates can be tuned in a programmable way. Active and even smart control of elastic waves are expected.

Conflicts of Interest

The authors declare that they have no known competing financial interests.

Data Availability Statement

Data in this article is available upon request.

Acknowledgments

The authors wish to thank Dr. Shuai Yang for his help in the numerical simulation. Financial supports by National Key R&D Program of China (2022YFB3806101), National Natural Science Foundation of China (12122207, 12021002, and 11991032) and the EIPHI

Graduate School (ANR-17-EURE-0002) are gratefully acknowledged.

---

† Electronic address: wangyanfeng@tju.edu.cn

[1] V. Laude. *Phononic Crystals: Artificial Crystals for Sonic, Acoustic, and Elastic Waves*. Walter de Gruyter GmbH, Berlin, 2015.

[2] M M Sigalas and E N Economou. Elastic and acoustic wave band structure. *Journal of Sound and Vibration*, 158:377–382, 1992.

[3] Manvir S Kushwaha, Peter Halevi, Leonard Dobrzynski, and Bahram Djafari-Rouhani. Acoustic band structure of periodic elastic composites. *Physical Review Letters*, 71(13):2022, 1993.

[4] Zhengyou Liu, Xixiang Zhang, Yiwei Mao, YY Zhu, Zhiyu Yang, Che Ting Chan, and Ping Sheng. Locally resonant sonic materials. *Science*, 289(5485):1734–1736, 2000.

[5] A Niousha and M Motosaka. Ground motion and structural vibration reduction using periodic wave barrier as a passive isolation. *WIT Transactions on the Built Environment*, 57:191–200, 2001.

[6] M B Assouar, M Senesi, M Oudich, M Ruzzene, and Z L Hou. Broadband plate-type acoustic metamaterial for low-frequency sound attenuation. *Applied Physics Letters*, 101:173505, 2012.

[7] Yi Zeng, Yang Xu, Keke Deng, Zuoxun Zeng, Hongwu Yang, Muhammad Muzamil, and Qiujiao Du. Low-frequency broadband seismic metamaterial using i-shaped pillars in a half-space. *Journal of Applied Physics*, 123(21):214901, 2018.

[8] Rosa Martinez-Sala, Constanza Rubio, Luis M Garcia-Raffi, Juan V Sanchez-Perez, Enrique A Sanchez-Perez, and J Llinares. Control of noise by trees arranged like sonic crystals. *Journal of Sound and Vibration*, 291:100–106, 2006.

[9] M Maldovan. Sound and heat revolutions in phononics. *Nature*, 503:209–217, 2013.

[10] Yan-Feng Wang, Vincent Laude, and Yue-Sheng Wang. Coupling of evanescent and propagating guided modes in locally resonant phononic crystals. *Journal of Physics D: Applied Physics*, 47:475502, 2014.

[11] M M Sigalas. Elastic wave band gaps and defect states in two-dimensional composites. *Journal of the Acoustical Society of America*, 101:1256–1261, 1997.

[12] M M Sigalas. Defect states of acoustic waves in a two-dimensional lattice of solid cylinders. *Journal of Applied Physics*, 84:3026–3030, 1998.

[13] Yinggang Li, Tianning Chen, Xiaopeng Wang, Ting Ma, and Ping Jiang. Acoustic confinement and waveguiding in two-dimensional phononic crystals with material defect states. *Journal of Applied Physics*, 116(2), 2014.

[14] M Torres, F R Montero de Espinosa, D Garcia-Pablos, and N Garcia. Sonic band gaps in finite elastic media: Surface states and localization phenomenain linear and point defects. *Physical Review Letters*, 82:3054–3057, 1999.

[15] A Khelif, A Choujaa, B Djafari-Rouhani, M Wilm, S Ballandras, and V Laude. Trapping and guiding of acoustic waves by defect modes in a full-band-gap ultrasonic crystal. *Physical Review B*, 68:214301, 2013.

[16] Soo-Ho Jo, Heonjun Yoon, Yong Chang Shin, Wonjae Choi, Choon-Su Park, Miso Kim, and Byeng D Youn. Designing a phononic crystal with a defect for energy localization and harvesting: Supercell size and defect location. *International Journal of Mechanical Sciences*, 179:105670, 2020.

[17] Liang-Yu Wu, Lien-Wen Chen, and Chia-Ming Liu. Acoustic energy harvesting using resonant cavity of a sonic crystal. *Applied Physics Letters*, 95(1), 2009.

[18] A Khelif, A Choujaa, S Benchabane, B Djafari-Rouhani, and V Laude. Guiding and bending of acoustic wavesin highly confined phononic crystal waveguides. *Applied Physics Letters*, 84:4400–4402, 2004.

[19] Xiaochun Li and Zhengyou Liu. Bending and branching of acoustic waves in two-dimensional phononic crystals with linear defects. *Physics letters A*, 338(3-5):413–419, 2005.

[20] Yan-Feng Wang, Ting-Ting Wang, Jun-Wei Liang, Yue-Sheng Wang, and Vincent Laude. Channeled spectrum in the transmission of phononic crystal waveguides. *Journal of Sound and Vibration*, 437:410421, 2018.

[21] I E Psarobas, N Stefanou, and A Modinos. Phononic crystals with planar defects. *Physical Review B*, 62:5536–5540, 2000.

[22] Y Pennec, B Djafari-Rouhani, J O Vasseur, A Khelif, and P A Deymier. Tunable filtering and demultiplexing in phononic crystals with hollow cylinders. *Physical Review E*, 69:046608, 2004.

[23] Y Pennec, B Djafari-Rouhani, J O Vasseur, H Larabi, A Khelif, A Choujaa, S Benchabane, and V Laude. Acoustic channel drop tunneling in a phononic crystal. *Applied Physics Letters*, 87:261912, 2005.

[24] Yan-Feng Wang, Ting-Ting Wang, Jin-Ping Liu, Yue-Sheng Wang, and Vincent Laude. Guid-

ing and splitting lamb waves in coupled-resonator elastic waveguides. *Composite Structures*, 206:588–593, 2018.

[25] Yan-Feng Wang, Yi-Ze Wang, Bin Wu, Weiqiu Chen, and Yue-Sheng Wang. Tunable and active phononic crystals and metamaterials. *Applied Mechanics Reviews*, 72(4):040801, 2020.

[26] X P Li, Y Y Chen, G K Hu, and G L Huang. A self-adaptivemetamaterial beam with digitally controlled resonators for subwavelengthbroadband flexural wave attenuation. *Smart Materials and Structures*, 27:045015, 2018.

[27] Li Ning, Yi-Ze Wang, and Yue-Sheng Wang. Broadband square cloak in elastic wave metamaterial plate with active control. *Journal of the Acoustical Society of America*, 150:4343, 2021.

[28] Gang Zhang and Yuanwen Gao. Tunability of band gaps in two-dimensional phononic crystals with magnetorheological and electrorheological composites. *Acta Mechanica Solida Sinica*, 34:40–52, 2021.

[29] Aichao Yang, Ping Li, Yumei Wen, Caijiang Lu, Xiao Peng, Jitao Zhang, Wei He, Decai Wang, and Chao Yang. Significant tuning of band structures of magneto-mechanical phononic crystals using extraordinarily small magnetic fields. *Applied Physics Letters*, 105:011904, 2014.

[30] Weirui Gao, Bin Yang, Ying Hong, Kai Guo, Peiqin Sun, and Jie Sun. Investigation on tunable low-frequency property of magnetic field induced phononic crystal with archimedean spiral-beams. *Mechanical Systems and Signal Processing*, 185:109756, 2023.

[31] Chunlong Gu and Feng Jin. Research on the tunability of point defect modes in a two-dimensional magneto-elastic phononic crystal. *Journal of Physics D: Applied Physics*, 49(17):175103, 2016.

[32] J Baumgartl, M Zvyagolskaya, and C Bechinger. Tailoring of phononic band structures in colloidal crystals. *Physical Review Letters*, 99:205503, 2007.

[33] K C Chuang, X F Lv, and D F Wang. A tunable elastic metamaterialbeam with flat-curved shape memory alloy resonators. *Applied Physics Letters*, 114:051903, 2019.

[34] Shuai Yang, Xiao-Liang Zhou, and Yan-Feng Wang. Tunable band gap and wave guiding in periodic grid structures with thermal sensitive materials. *Composite Structures*, 190:115536, 2022.

[35] Heng Liu, Shao-yong Huo, Lu-yang Feng, Hong-bo Huang, and Jiu-jiu Chen. Thermally tunable topological edge states for in-plane bulk waves in solid phononic crystals. *Ultrasonics*, 94:227–

234, 2019.

[36] Ting-Ting Wang, Yan-Feng Wang, Yue-Sheng Wang, and Vincent Laude. Tunable fluid-filled phononic metastrip. *Applied Physics Letters*, 111(4):041906, 2017.

[37] T T Wang, Y F Wang, Z C Deng, V Laude, and Y S Wang. Wave propagation in coupled-resonator acoustoelastic waveguides. *Composite Structures*, 303:116355, 2023.

[38] E. Kim, A. J. Martinez, S. E. Phenisee, P. G. Kevrekidis, M. A. Porter, and J. Y. Yang. Direct measurement of superdiffusive energy transport in disordered granular chains. *Nature Communications*, 9:640, 2018.

[39] F Allein, V Tournat, VE Gusev, and Georgios Theocharis. Tunable magneto-granular phononic crystals. *Applied Physics Letters*, 108(16), 2016.

[40] Massimiliano Gei, AB Movchan, and Davide Bigoni. Band-gap shift and defect-induced annihilation in prestressed elastic structures. *Journal of Applied Physics*, 105(6):063507, 2009.

[41] Y. Z. Wang, F. M. Li, K. Kishimoto, Y. S. Wang, and W. H. Huang. Band gaps of elastic waves in three-dimensional piezoelectric phononic crystals with initial stress. *European Journal of Mechanics A-Solids*, 29:182, 2010.

[42] Hai-Fei Zhu, Xiao-Wei Sun, Ting Song, Xiao-Dong Wen, Xi-Xuan Liu, Jin-Shan Feng, and Zi-Jiang Liu. Tunable characteristics of low-frequency bandgaps in two-dimensional multivibrator phononic crystal plates under prestrain. *Scientific Reports*, 11(1):1–12, 2021.

[43] Z N Li, Y Z Wang, and Y S Wang. Tunable nonreciprocal transmissionin nonlinear elastic wave metamaterial by initial stresses. *International Journal of Solids and Structures*, 182-183:218–235, 2020.

[44] Rongxin Feng and Kaixin Liu. Tuning the band-gap of phononic crystals with an initial stress. *Physica B: Condensed Matter*, 407(12):2032, 2012.

[45] K Bertoldi and M C Boyce. Mechanically triggered transformations of phononic band gaps in periodic elastomeric structures. *Physical Review B*, 77(052105), 2008.

[46] K Bertoldi and M C Boyce. Wave propagation and instabilities in monolithic and periodically structured elastomericmaterials undergoing large deformations. *Physical Review B*, 78(184107), 2008.

[47] S. Shan, S. H. Kang, P. Wang, C. Qu, S. Shian, E. R. Chen, and K. Bertoldi. Harnessing multiple folding mechanisms in soft periodic structuresfor tunable control of elastic waves. *Advanced Functional Materials*, 24:4935–4942, 2014.

[48] Atul Kumar Sharma, M.M. Joglekar, D.M. Joglekar, and Zeeshan Alam. Topology optimization of soft compressible phononic laminates for widening the mechanically tunable band gaps. *Composite Structures*, 289:115389, 2022.

[49] A. Bayat and F. Gordaninejad. Switching band-gaps of aphononic crystal slab by surface instability. *Smart Materials and Structures*, 24(075009), 2015.

[50] Y. J. Chen, B. Wu, Y. P. Su, , and W. Q. Chen. Tunable two-wayunidirectional acoustic diodes: Design and simulation. *Journal of Applied Mechanics*, 86(031010), 2019.

[51] R De Pascalis, T Donateo, A Ficarella, and W J Parnell. Optimal design of phononic media through geneticalgorithm-informed pre-stress for the control of antiplane wave propagation. *Extreme Mechanics Letters*, 40:100896, 2020.

[52] M. Miniaci, M. Mazzotti, A. Amendola, and F. Fraternali. Effect of prestress on phononic band gaps induced by inertial amplification. *International Journal of Solids and Structures*, 216:156–166, 2021.

[53] K. Bertoldi, V. Vitelli, J. Christensen, , and M. van Hecke. Flexible mechanical metamaterials. *Nature Reviews Materials*, 2(17066), 2017.

[54] Yueting Wang, Jian Li, Yuxin Fu, Ronghao Bao, Weiqiu Chen, and Yue-Sheng Wang. Tunable guided waves in a soft phononiccrystal with a line defect. *APL materials*, 9(051124), 2021.

[55] Yan-Feng Wang, Ting-Ting Wang, Jin-Ping Liu, Yue-Sheng Wang, and Vincent Laude. Guiding and splitting lamb waves in coupled-resonator elastic waveguides. *Composite Structures*, 206:588–593, 2018.

[56] Yan-Feng Wang, Li Yang, Ting-Ting Wang, A-Li Chen, Vincent Laude, and Yue-Sheng Wang. Guided lamb waves in reconfigurable phononic crystal waveguides. *APL Materials*, 9(8):081110, 2021.

[57] Jie Wang, Jin Di, Qian Zhang, and Fengjiang Qin. Overall buckling behaviour of q420–q960 steel welded h-section axial compression members. *Engineering Structures*, 249:113340, 2021.

[58] H Jiao and X.-L Zhao. Imperfection, residual stress and yield slenderness limit of very high strength (vhs) circular steel tubes. *Journal of Constructional Steel Research*, 59(2):233–249, 2003.

[59] K.J.R. Rasmussen and G.J. Hancock. Tests of high strength steel columns. *Journal of Constructional Steel Research*, 34(1):27–52, 1995.

[60] Yan-Feng Wang, Ting-Ting Wang, Yue-Sheng Wang, and Vincent Laude. Reconfigurable

phononic crystal circuits formed by coupled acoustoelastic resonators. *Physical Review Applied*, 8:014006, 2017.